COMMUN. MATH. SCI.
Vol. 17, No. 5, pp. 1387–1406

THE EVOLUTION OF LARGE-SCALE MODELING OF MONKEY PRIMARY VISUAL CORTEX, V1: STEPS TOWARDS UNDERSTANDING CORTICAL FUNCTION*

LAI SANG YOUNG†, LOUIS TAO‡, MICHAEL SHELLEY§, ROBERT SHAPLEY¶, AADITYA RANGAN‖, AND DAVID W. MCLAUGHLIN**

In memory of Professor David Shenou Cai

Abstract. Over the past two decades, mathematicians and neuroscientists at New York University have developed several large-scale computational models of a layer of macaque primary visual cortex. Here we provide an overview of these models, organized by the specific questions about cortical processing that each model addressed. Each model was founded upon the available anatomical and physiological data; and not by building into the model network assumptions about theoretical mechanisms specifically designed to enable the network to produce desired response properties. Also, our aim was to use one comprehensive network, with a fixed architecture and one set of parameters, to model all experiments. The response properties of individual neurons and populations of neurons then emerge from this experimentally constrained model. This overview is dedicated to Professor David Cai, who played a leading role in several of the models described here. We are very fortunate to have had the opportunity to work with him over the past two decades.

Keywords. Visual Neural Science; Computational Modeling; Orientation Tuning.

AMS subject classifications. 60F10.

1. Introduction

What are the purposes and general goals of large-scale computational modeling in neural science? What are the problems to be solved and the questions to be answered? Perhaps the first, most basic question is: "Is enough known from experiments on the brain area, in sufficient detail, to construct a large scale model that emulates that area's function?"

The macaque monkey's primary visual cortex (V1), and especially an input layer of V1 such as 4Cα, seems a good place to start to answer the basic question with large-scale cortical modeling. V1, the cortical "front end" of the visual pathway (Retina $\rightarrow$ LGN $\rightarrow$ V1 $\rightarrow$ higher cortical areas), is the first cortical area within which significant visual processing is known to take place. Its input from the Lateral Geniculate Nucleus (LGN) is well-characterized. Its input layer 4Cα receives minimal feedback from higher cortical areas. In addition, there is a large amount of experimental data about V1 - far more than for other cortical areas.

*Received: April 2, 2019; Accepted (in revised form): September 6, 2019.

†Courant Institute of Mathematical Sciences, New York University, 251 Mercer Street, New York (NY) 10012, USA (lsy@cims.nyu.edu).

‡Center for Bioinformatics, National Laboratory of Protein Engineering and Plant Genetic Engineering, School of Life Sciences, Peking University, Beijing, 100871, China; Center for Quantitative Biology, Peking University, Beijing, 100871, China (taolt@mail.cbi.pku.edu.cn).

§Courant Institute of Mathematical Sciences, New York University, 251 Mercer Street, NY 10012, USA; and Simons Foundation, 160 Fifth Ave, NY 10010, USA (shelley@cims.nyu.edu).

¶Center for Neural Science, Courant Institute of Mathematical Sciences and Neuroscience Institute at NYU Langone Medical Center, New York University, 4 Washington Place, NY 10003, USA (shapley@cns.nyu.edu).

‖Courant Institute of Mathematical Sciences, New York University, 251 Mercer Street, NY 10012, USA (rangan@cims.nyu.edu).

**Courant Institute of Mathematical Science, Center for Neural Science, Tandon School of Engineering, Neuroscience Institute at NYU Langone Medical Center, New York University, 251 Mercer Street, NY 10012, USA (david.mclaughlin@nyu.edu).

Our work on models of V1 was stimulated by Sompolinsky's "ring model" [1] for orientation selectivity that captured the cortex's sharpening of untuned input from LGN. But the ring model is a heuristic model - a ring of neurons. There is no "ring" in V1; rather, neurons in V1 reside in two dimensional cortical surfaces or layers. Could one simulate the cortex with a model of V1 as a surface of neurons? If so, it would necessitate large-scale modeling because of the number of neurons in the surface, even just in the input layer.

The co-authors of this overview article have developed several different large-scale models of a layer of macaque V1 [2–7, 9, 27, 32]. We have used each model to answer specific questions about cortical processing. The overriding theme that links much of the work presented here is the importance of recurrent cortical-cortical connections between neurons in determining the responses of cortical neurons.

Before describing the various models, we want to express explicitly the modeling philosophy that guided much of this work. Our philosophy of large-scale modeling is founded upon using experimental anatomical and physiological data to guide the design of models. One does NOT build into the model network assumptions about theoretical mechanisms that are designed to enable the network to yield desired response properties. The response properties of individual neurons and those of the full neuronal network then emerge from this experimentally constrained construction. Also, our aim was to use one network, with a fixed architecture and one set of parameters, to model many experiments. Each of the models reviewed here aimed to be comprehensive, that is, one model with one set of parameters had to fit many functional data. This was the only satisfactory path to answer the fundamental question: Is what we know from experiments enough to enable us to emulate the cortex?

If the response properties of a large-scale model agree with the biological responses of the brain area, one can then use analytical "post-processing" techniques to identify precisely the mechanisms by which the model achieves its responses. Understanding the mechanisms in the model can lead to insights about mechanisms in the real cortex by making predictions that can be tested by data from new experiments.

The paper is organized as follows: First, we present a description of the general model architecture that is shared among models. Then we discuss each model, and the questions that we asked and answered with that model.

2. General model architecture

Each of our models belongs to a general class of model neuronal networks: large-scale recurrent networks of spiking neurons, conductance based with high network conductances, with strong synaptic connectivity, strong nonlinear dynamics, exhibiting complicated high-order neuronal interactions – models that cannot be easily "coarse-grained". But the individual models are very different from each other; for example, they have crucial different internal balances that result in important differences in their dynamics. Here we begin with a description of the common generic architecture of the models. In the specific models discussed later, different investigators made many different choices of connectivity and parameters, which will be discussed as they are presented.

The generic model represents a $1mm^2$ local patch of input layer $4C\alpha$, modeled as conductance based, "integrate and fire" (I&F) point neurons. The model is a coupled system of many point neurons (75% of which are excitatory and 25% inhibitory, approximating the real cortex), represented as a system of equations for $V_\sigma^j(t)$, the j^{th}

neuron's membrane potential:

$$C\frac{d}{dt}V_\sigma^j = -g_L\left(V_\sigma^j - E_L\right) - g_{\sigma E}^j(t)\left[V_\sigma^j - E_E\right] - g_{\sigma I}^j(t)\left[V_\sigma^j - E_I\right]. \tag{2.1}$$

Here $j=(j_1,j_2)$ labels the neuron's location within the patch, $\sigma=(E,I)$ labels the neuron's type (excitatory or inhibitory). The functions $g_{\sigma E}^j(t), g_{\sigma I}^j(t)$ denote the temporal profiles of the excitatory (inhibitory) conductances that impinge upon the j^{th} neuron of type σ. The spike times are denoted by $t_l^{\sigma j}$, the l^{th} spike time of the jth neuron of type σ. When the voltage $V_\sigma^j(t=t_l^{\sigma j})$ reaches spiking threshold V_T, the spike time $t_l^{\sigma j}$ is recorded, the voltage is reset to E_R, held there for a brief time t_R, and then re-initialized as $V_\sigma^j(t=t_l^{\sigma j}+t_R)=E_R$. The capacitance C, "leak conductance" g_L, the reversal potentials (E_L,E_E,E_I) are constants, as is the threshold V_T. The "refractory period" $t_R=2ms(1ms)$ for (inhibitory) neurons. We used commonly accepted values for the biophysical parameters $C=10^{-6}Fcm^{-2}, g_L=50\times10^{-6}\Omega^{-1}cm^{-2}$, and $E_I(-80mv)<E_L(-70mv)<V_T(-55mv)<E_E(0mv)$.

The conductances in Equation (2.1) drive the time evolution of the membrane voltage. The *excitatory conductance* is given by

$$\begin{aligned} g_{\sigma E}^j(t) &= g_{lgn}^j(t) + g_{cort-cort,E}^j(t) + \nu_E^j(t), \\ g_{cort-cort,E}^j(t) &\equiv S_{\sigma E}\sum_{k,l}[K_{j-k}^{\sigma E}G_E(t-t_l^{E,k})], \end{aligned} \tag{2.2}$$

and the *inhibitory conductances* by

$$\begin{aligned} g_{\sigma I}^j(t) &= g_{cort-cort,I}^j(t) + \nu_I^j(t), \\ g_{cort-cort,I}^j(t) &\equiv S_{\sigma I}\sum_{k,l}[M_{j-k}^{\sigma I}G_I(t-t_l^{I,k})]. \end{aligned} \tag{2.3}$$

The temporal profiles of both the excitatory and inhibitory cortical-cortical conductances, Equation (2.2), (2.3), were derived from cortical data. The LGN conductance in Equation (2.2) is the sum of synaptic conductance waveforms evoked by LGN spikes, with kinetics like the conductance waveforms of cortico-cortical synapses. Each LGN neuron's spike train is modeled as a modulated Poisson process. The modulation of the spike rate of the k^{th} LGN neuron is computed as a rectified space-time filter of the visual stimulus $I(x,t)$:

$$R_\pm^k(t) = \left\{R_B \pm \int\int G(t-s)A(|x_k-x|)I(x,s)d^2xds\right\}^+, \tag{2.4}$$

where $I(x,t)$ denotes the visual stimuli. For example in the case of drifting gratings, $I(x,t)$ takes the form $I(x,t)=I_0[1+\epsilon\sin(k\cdot x-\omega t-\phi)]$, with parameters I_0 (mean light intensity), ϵ (contrast), ω (temporal frequency), ϕ (spatial phase), $k=|k|[\cos(\theta),\sin(\theta)]$ (with $|k|$ the spatial frequency and θ the orientation of the grating). R_B denotes the spontaneous firing rate of individual LGN neurons. $A(|x_k-x|)$ is a circularly-symmetric difference of Gaussians, centered in visual space on the receptive field location x_k of each LGN neuron in visual space. The two possible signs before the integrals in Equation (2.4) capture the duality of LGN cells; namely, whether the cell responds to an increase in luminance at the center of the receptive field, and to a decrease in luminance in the surround (an "on-center LGN cell"); or vice-versa (an "off-center LGN cell"). The

temporal profile $G(t-s)$ in Equation (2.4) was derived from experimental data on LGN neurons [11].

The receptive field of each cortical cell was spatially larger than that of each of its LGN components; it had a "sub-field" structure that provided each V1 cell with its orientation preference for the orientation of edges in the visual scene. In different models, the number of LGN neurons projecting to a given cortical neuron (N_{LGN}) was different.

Experimental data indicate that V1 has a orientation columnar structure, with each cortical layer tiled by an ordered map of orientation preference, with each Hypercolumn (HC) "tile" approximately 0.5 mm x 0.5mm in spatial extent. In most models the density of cells was 4,000 cells/tile (4 tiles total), a number dictated by anatomical data [12]. Within a tile, the orientation preferences conferred by the LGN input to the cortex changed smoothly around the "pinwheel singularity" at the center of each tile. The ordered "pinwheel tiling" of oriented LGN input was built into the models.

In addition to orientation preference, V1 neurons also have spatial and temporal phase preferences. These were not ordered within the pinwheel tiling; rather they are observed experimentally to be random. These random phase preferences were put into the model through the LGN inputs as described above for orientation preference.

The spatial kernels $K^{\sigma E}_{j-k}$ and $M^{\sigma I}_{j-k}$ in Equation (2.2), (2.3) represent the spatial pattern of coupling between neurons, taken to be isotropic Gaussians with length scales of 200 μm for excitation and 100-200 μm for inhibition, consistent with anatomical studies. All kernels were normalized to unity; hence, the coupling strengths were solely described by the coupling matrix $S^{\alpha}_{\sigma\sigma'}$ in Equation (2.2), (2.3).

In early models, the cortical-cortical coupling was "all to all", with coupling strengths falling off as a Gaussian with distance. Later proposed models had significantly sparser excitatory and inhibitory connectivity. The nature of the sparsity of connections and the dependence of synaptic coupling with distance was handled differently in different later models.

Finally, $\nu^j_E(t)$ and $\nu^j_I(t)$ in Equation (2.2), (2.3) are noise terms representing inputs from other cortical layers and areas,

$$\nu^j_\sigma(t) \equiv S^\nu_\sigma \sum_l G_\sigma(t-s_l), \sigma = E, I, \tag{2.5}$$

with the spike times s_l a Poisson process with rate $\nu^j_\sigma(t)$ chosen to ensure that the model cortical neurons had a range of spontaneous firing rates like those observed in V1.

The general question we sought to answer was whether or not this generic model architecture, with local isotropic cortico-cortical connectivity, was sufficient to model the input layer of the real cortex. In many specific models developed later the answer seems to be "yes" but with qualifications, as explained in the body of the paper.

3. Specific large-scale V1 models

3.1. Earliest large-scale V1 model. To begin, in [2, 3] the authors posed the following questions: **Orientation selectivity:** Individual cortical cells possess orientation preference and orientation selectivity. Orientation preference is set by the orientation maps of feed forward connection properties of the group of LGN neurons projecting to the given cortical neuron. However, orientation selectivity of some cortical neurons is much greater than that of the summed input from neurons in the Lateral Geniculate Nucleus (LGN), as established in [13], among others. These results led to the first questions:

- How does the full cortical network cause and shape orientation selectivity, and its distribution over neurons?
- What are the roles of cortical excitation and inhibition?

Dynamics – time course of orientation tuning: Rapid presentation of flashed patterns and reverse correlation of the stimulus patterns with V1 spike trains revealed that orientation tuning occurred rapidly in V1 neurons.

- Can the model explain reverse correlation data on the time course of orientation tuning?

Existence of simple cells: Individual cells in the cortical layer respond to visual stimuli with varying degrees of linearity. Some cells, called simple cells, respond linearly while others, called complex cells, respond very nonlinearly with distorted wave forms containing multiple harmonics. It is surprising that linear (simple) cells exist at all, given the nonlinearities of the LGN and cortical-cortical excitatory drives.

- Do simple cells exist in the model cortical network; and, if so, how do these linear response properties emerge in the model?

To answer these questions about cortical function, [2] devised the earliest large-scale model of layer $4C\alpha$ of V1 that we are summarizing. That model generally resembled the model template described in Section 2. It was a model of a local patch of input layer $4C\alpha$, representing $1mm^2$ (four orientation pinwheels) containing $\sim 16{,}000$ neurons (75% excitatory and 25% inhibitory). In this model, on average 17 LGN neurons made excitatory synapses on each cortical neuron, following the interpretations of experimental data by Alonso, et al. [22]. These collections produced a relatively strong summed LGN input to most cortical cells. The LGN input imparted orientation preference and weak orientation selectivity. The model's recurrent cortico-cortical coupling was "all to all", with the synaptic arbors drawn isotropically in cortical space, without any explicit spatial bias regarding the postsynaptic orientation-preference. The model operated with high conductances that resulted primarily from high inhibitory conductance. In summary, the model was dominantly feed-forward with relatively weak recurrent excitation, but it had strong recurrent inhibition.

3.1.1. Question 1: Orientation selectivity of cortical neurons. Many neurons in V1 cortex respond best to a particular orientation of edges in the visual scene. For each V1 neuron, one can measure an orientation tuning curve, a graph of the neuron's firing rate vs. the orientation of the visual stimulus. There are two aspects of orientation tuning: preference and selectivity. Measured V1 tuning curves usually are uni-modal, with peak at "preferred orientation" and trough at the orientation orthogonal to preferred. A neuron's "orientation selectivity" is how much more the neuron responds to stimuli at its optimal orientation compared to other orientations. Measures of orientation selectivity include the curves' "half width" (also called bandwidth). However, there are alternative measures such as circular variance (CV) that compare the response at the preferred orientation to responses at all orientations including at orthogonal. Sharply tuned neurons have a CV near 0, while CV's of broadly-tuned neurons are near 1 [19].

In the vintage 2000 model, the dominance of inhibition in the recurrent cortical-cortical activity provides the mechanism that causes and shapes the model population's orientation selectivity. Inhibition, the summed inhibitory current from all inhibitory neurons that make synaptic connections on a neuron, is more broadly orientation-tuned than excitation. This broad (or global) inhibition shapes the tuning curves by bringing down the firing rates near orthogonal (far from orientation preference). Figure 3.1 shows

the comparison of the model's orientation selectivity with that of experiment. There is good qualitative agreement between model and data in Figure 3.1; in particular the model does generate some sharply tuned cells. Figure 3.1b also displays the predicted orientation tuning curve of the feedforward LGN current, as a dashed curve. The feedforward input is substantially less selective than the most highly selective cortical cells, indicating the important role of the cortical network in orientation selectivity.

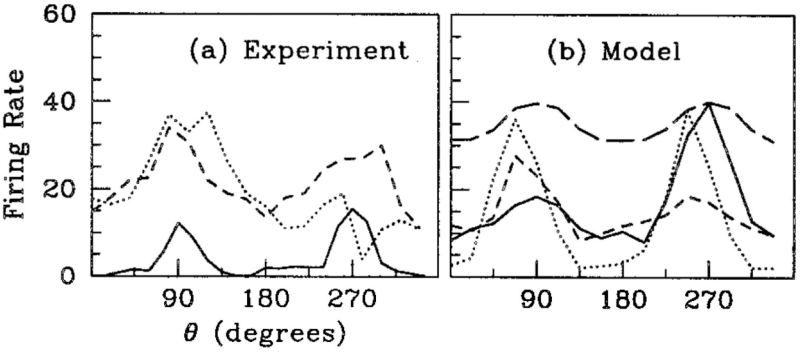

FIG. 3.1. **Sample Orientation Tuning Curves from Drifting Grating Stimuli:** *(a) Experiment (three sample cells). The response is measured as the time-averaged firing rate and is plotted in units of spikes per second. Stimuli were at optimal temporal frequency for each neuron, 2-10 Hz. (b) Model (excitatory neurons, simulated at 8 Hz). The model results also include the orientation selectivity obtained by an uncoupled neuron (long-dash line, the "feed-forward" response), normalized for comparison to a peak response of 40 spikes per second. Reprinted from Proc. Nat. Acad. Sci. (USA), ref [2].*

3.1.2. Question 2: Dynamics of orientation preference and selectivity. Does the large-scale model [2] capture the dynamical behavior of orientation preference and selectivity? Dynamical behavior is measured experimentally by reverse time correlation (RTC) experiments [18]. In reverse correlation experiments, visual stimuli, randomly-oriented stationary gratings, are flashed and then refreshed every 17 ms, with each pattern taken randomly and independently from a collection of patterns with N values of orientation $\{\theta = 2k/N, k = 1,2,,N\}$ and M values of the phase $\{\phi = 2k/M, k = 1,2,,M\}$. Spike times of a given cortical neuron are correlated with previous visual stimuli to measure $P(\theta,\tau)$, the probability that τ ms before a spike is fired, visual stimulation at orientation θ occurred.

Figure 3.2 displays the temporal evolution of $P(\theta,\tau)$ for both experimental and model data, showing qualitative agreement between the two. Also shown is the circular variance of $P(\theta,\tau)$, $CV[P]$, as a function of τ which captures the temporal time course of orientation selectivity – the model is in rough agreement with experiment.

3.1.3. Question 3: Existence of simple cells. Previously visual spatial summation was studied with particular visual stimuli: contrast reversal gratings, [20, 21]. Such stimuli also were effective for classifying cells as simple or complex. Simple cells respond to contrast reversal gratings at the fundamental frequency of temporal modulation ω, with small amplitudes of second (or higher) temporal harmonics, while complex cells would respond to contrast reversal with large second harmonics at many different spatial phases. Each simple cortical cell is driven by the summed excitatory input from the LGN, which has significant frequency doubling (second harmonic). And yet, there were many simple cells in the model. How did this happen?

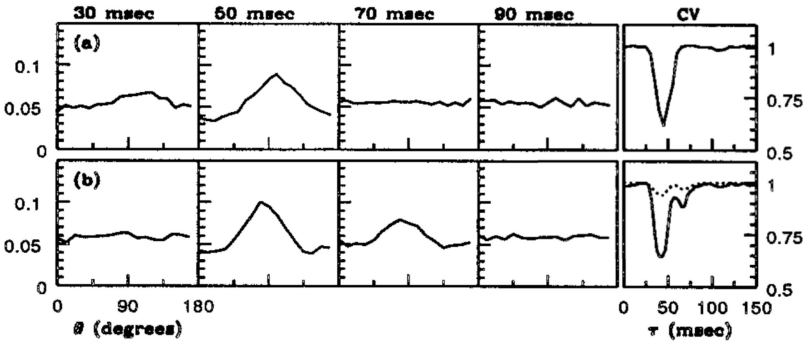

FIG. 3.2. $P(\theta,\tau)$ **from RTC at Several Times τ, Showing the Dynamics and Sharpening of Orientation Selectivity:** *The normalized correlation, $P(\theta,\tau)$, is the probability that τ msec before a spike was produced, an image with angle θ was presented. The graph's left vertical scale is probability, whereas the vertical scale on the right, for the rightmost boxes only, is in units of CV. (a) Experiment (4Cα simple cell, 18 angles). (b) Model (16 angles). The rightmost boxes show circular variance $CV[P(\cdot,\tau)]$. The dashed CV[P] curve in (b) is that for an uncoupled model neuron, and it shows that feed-forward input by itself produces only a small reduction in CV in the RTC experiment. Reprinted from Proc. Nat. Acad. Sci. (USA), ref [2].*

The key to the existence of simple cells is cortical interactions. In addition to being driven by LGN spike trains, cortical cells are excited by spike activity in nearby excitatory cells and inhibited by spikes in nearby inhibitory cells. Spikes from the LGN and from cortical cells influence a target cell through their synaptic conductances. Cortical neurons sum all the incoming synaptic conductances. This summation effectively averages the phases of the responses from the different neighboring neurons, producing significant second harmonics in the cortical-cortical excitatory and inhibitory drive. But in the early model [2], inhibition is large, and the inhibitory second harmonic terms cancel the excitatory second harmonics in the LGN drive and also in the weaker cortical-cortical excitation; thus, simple, linear cells emerge in the model because of the cancellation of excitatory harmonic distortion by inhibitory harmonic distortion.

This early model provided the first explanation, based upon cortical architecture, for the existence of simple cells [3].

3.2. The egalitarian model. In the classical model of Hubel and Wiesel [10], V1 simple and complex cells are part of a feed-forward hierarchy: simple cells receive strong geniculate excitation and pool their outputs to drive complex cells. Therefore, in response to sinusoidally-modulated, drifting gratings, a simple cell responds linearly by following the temporal modulation of the grating and peaks when its receptive field and the stimulus maximally overlap. A complex cell, by pooling many different phase-specific simple-cell outputs, responds with a temporally unmodulated firing rate. To classify the simple/complex responses of individual V1 cells, [18] analyzes the response modulation to the drifting grating stimulus. They find that many V1 cells are neither wholly simple nor wholly complex but lie somewhere in between. Simple and complex cells appear in roughly equal proportion.

The earlier 4Cα model produced a V1 network entirely of simple cells. How can one incorporate complex cells in this model and so explain how the observed distribution of simple and complex cells arises in the cortex?

3.2.1. Question: The distribution of simple and complex cells. Individual V1 cells respond with varying degrees of linearity. In [3], simple cell responses

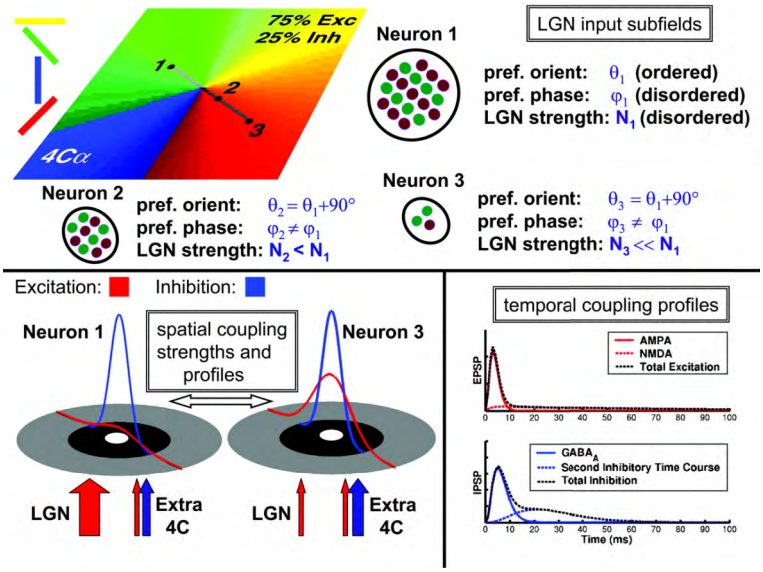

FIG. 3.3. **Schematic of the Egalitarian model:** *Upper panel: Inputs from the visual stimulus, as relayed through the LGN. Each V1 neuron receives (excitatory) visual stimulation through a collection of LGN cells that is probabilistically chosen from a two-dimensional Gabor function. Orientation preference is laid out in pinwheels (color map) and the spatial phase preference is distributed randomly (map not shown, but examples are shown for 3 neurons). Lower left: Intracortical couplings are isotropic and are modeled to be Gaussians in space (excitation in red and inhibition in blue). Lower right: Each cortico-cortical postsynaptic conductance is modeled as a single or a sum of alpha functions. Reprinted from [4].*

are produced by the feed-forward excitation of its presynaptic LGN neurons and the phase-invariant inhibition produced by the cortical network of simple cells. However, the cortico-cortical excitatory conductance of each neuron resembles the responses of complex cells. These results led to the questions:

- How do individual simple and complex cells arise in the network?
- How does the network shape the simple and complex cell distribution in cortex?
- What are the roles of feed-forward excitation, and of cortical excitation and cortical inhibition?

To address these questions, Tao *et al.* [4] studied a 4Cα network where each neuron receives excitatory drive from a widely varying number of presynaptic LGN cells. Lacking evidence that cortical inhibition differs widely in 4Cα neurons, cortical inhibitory coupling strengths are assumed uniform across the network. This leads to the central assumption of our *Egalitarian* model: the total excitation, divided between geniculate and cortical, is roughly constant.

Mathematically, the Egalitarian model consists of the systems of I&F point neurons, Equations (2.1), (2.3)-(2.5); a schematic of the model is shown in Figure 3.3. The collective LGN drive into a single V1 neuron is modeled as a Poisson spike train whose time-varying rate is a sum of linear spatiotemporal filters. The on- and off-centered LGN cells presynaptic to a V1 neuron are segregated into elongated Gabor-like subregions, tilted at a preferred angle and having a preferred spatial phase. As in the earlier models, preferred orientation is laid out in pinwheel patterns, while preferred spatial phase varies randomly from neuron to neuron. In a difference from the earlier models, the number

of LGN cells presynaptic to a V1 neuron is distributed randomly, with that number being independent from neuron to neuron. In particular, some cortical cells receive significant LGN drive while their neighbors may receive little or no LGN excitation. We combine this with the constraint that the total excitatory synaptic drive onto each cell is approximately constant, with those neurons receiving weak or no LGN drive receiving stronger recurrent excitation.

Having already explained how simple cells arise in a network of simple cells, let us consider how a complex cell might arise in the egalitarian network. Consider a V1 neuron receiving little or no LGN input but is driven strongly by cortico-cortical inputs. In a network of simple and complex cells, a contrast-reversing grating over one cycle of stimulation would drive neurons with different spatial phase preferences, and a non-specific pooling of these neurons' outputs would produce synaptic inputs that are frequency doubled and insensitive to spatial phase.

The trade-off between LGN and cortico-cortical drive is key to how the egalitarian model produces both simple and complex cells.

3.2.2. Simple and complex cells under drifting gratings. Let us now examine the case of drifting grating stimulus, which also evokes differences between simple and complex cells. For the model's simple and complex cells, Figure 3.4 shows their firing rate and membrane potential responses to a drifting grating. The simple cell follows the temporal modulation of the grating whereas the complex cell responds in an elevated, mostly constant fashion. Figure 3.4 shows that the strong LGN excitation into the simple cell follows the stimulus frequency. In the network, different cells have differing spatial preference and receive diverse LGN excitation, and so their outputs are diverse in both amplitude and time of peak excitation. Pooling their responses yields nearly time-invariant cortico-cortical conductances. Thus, for the model simple cell, both the intracellular effective reversal potential, V_S, and its extracellular firing pattern modulate on the time dependence of its LGN input. For the model complex cell both V_S and the firing pattern are driven by the steady cortico-cortical conductances, and show only elevated, unmodulated responses. Therefore, in the egalitarian network, drifting gratings evoke a spectrum of balances between LGN and cortico-cortical forcing, having phase specific cells whose firing follows the temporal modulation of the grating, cells with phase insensitive firing, and cells a mixture of both.

3.2.3. Population distributions of modulation ratio. The two cells examined in Figure 3.4 are examples from a continuum of intracellular and extracellular responses that reflects the trade-off between LGN and cortico-cortical drive. We explore this continuum further for drifting grating stimulus using the *modulation ratio* F_1/F_0, which is, given a periodic response at the stimulus frequency, the ratio of the first harmonic amplitude to the mean. Complex cells have modulation ratios near zero; their responses are nearly constant in time (Figure 3.4b), while simple cells, whose responses modulate with the stimulus, have modulation ratios near two (Figure 3.4a). Figure 3.5a shows the histogram of F_1/F_0 for the cycle-averaged effective reversal potential, V_S, across the whole cortical population. The distribution is broad, unimodal, and monotonically decreasing, and reflects the broad distribution in number of LGN afferents and the constraint of fixed total synaptic excitation within the model. Experimental measurements [17] show also a broad and unimodal distribution of the membrane potential's F_1/F_0. This unimodality is not preserved in F_1/F_0 distribution of the firing rate. Figure 3.5b shows the distribution of modulation ratio of the cycle-averaged firing rate. Qualitatively similar, the distributions from both model and experiment show a bimodal structure peaked near the extremes of the classifier, but still with a large pro-

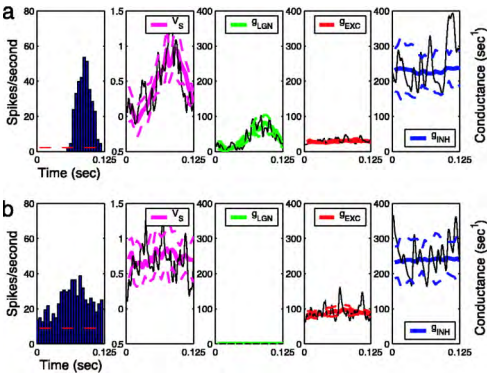

FIG. 3.4. **Responses to drifting gratings:** *(a) The model simple cell. (b) The model complex cell. From left to right: cycle-averaged firing rates (spontaneous rates as dashed red lines); effective reversal potential V_S (magenta); LGN-driven conductance (green); cortico-cortical excitatory conductance (red); cortico-cortical inhibitory conductance (blue). The dotted lines are standard deviations. The thin black lines indicate instantaneous values of conductances and potentials. Reprinted from [4].*

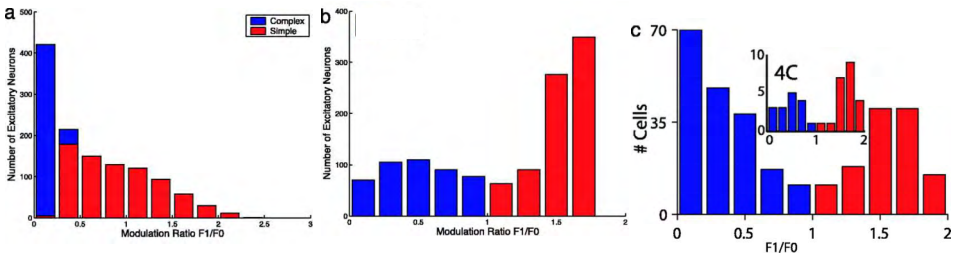

FIG. 3.5. **Modulation Ratio:** *(a) Distribution of F_1/F_0 of membrane potential of excitatory neurons in model network. (b) Distribution of F_1/F_0 of the firing rate for excitatory neurons in model network. (The distribution for the inhibitory population is qualitatively similar.) For these two distributions, only cells with mean rates greater than 8 spikes per sec are included. (c) Distribution of the modulation ratio F_1/F_0 of the firing rate for 308 cells (complex cells, $n = 184$; simple cells, $n = 124$) from the experiments of Ringach et al. [18]. Reprinted from [4].*

portion of cells having responses that are neither wholly simple, nor wholly complex. Mechler and Ringach [15] have shown that spike-rate rectification could be responsible for transforming a unimodal membrane potential F_1/F_0 distribution into a bimodal distribution in firing rate F_1/F_0 (see also [16]). Figure 3.4 shows that this result is a natural consequence of the highly diverse balance between LGN and cortico-cortical synaptic drives in the egalitarian model.

3.3. Sparse, high gain model. *Orientation Selectivity of Complex Cells:* While the egalitarian model had reasonable distributions of simple and complex cells, its complex cells were poorly tuned, and not as selective for orientation as experimentally observed. Thus, the question:

- Can a model be developed, realistically constrained by experimental observations, the complex cells of which are sufficiently orientation selective?

A High Gain Stable Network: In order for sufficiently selective complex cells to emerge in the egalitarian model, it seemed that much stronger cortical-cortical excitation was needed. However, as cortical excitation was increased, the model quickly went unstable, with firing rates that were much too high (limited only by the refractory period). Hence,

three overriding questions:

- Does a "high-gain" network exist with strong cortical-cortical excitation, which is stable with reasonable firing rates?
- What are the mechanisms that stabilize the network?
- What are the characteristics of the "operating point" or "operating state" of this model cortical network?

The model developed in [5] is very similar to the egalitarian model [4], although with the network architecture simplified slightly. The main difference is that its excitatory connections are *sparse* and much *stronger*. These are introduced into the model by hardwiring randomly: Let p_k^j denote the probability that neuron k is connected to neuron j. p_k^j is chosen, independently for each j and k, to be 1 with probability p and 0 otherwise. This fixes the connectivity once and for all – a connectivity in which all neurons, regardless of E or I type, have the same average degree of sparsity. Thus, on average each neuron will be connected to $N_{eff} = pN$, where N is the total number of neurons in the network. The conductances are then scaled by the factor p_k^j/p:

$$g^j_{cort-cort,E}(t) \equiv S_{\sigma E} \sum_{k,l} \left[\left(\frac{p_k^j}{p} \right) K^{\sigma E}_{j-k} \left[(1-\Lambda) G_E^{AMPA}(t - t_l^{E,k}) + \Lambda G_E^{NMDA}(t - t_l^{E,k}) \right] \right]. \tag{3.1}$$

Note that the probability $p \in [0,1]$ controls the mean connectivity, with small p sparse and $p = 1$ all to all; also, p^{-1} scales up the strength of the individual connections, making sparser networks have stronger postsynaptic conductances (PSCs). In addition as in [4], NMDA conductances are added to the much faster AMPA conductances, with the parameter Λ representing the % of NMDA. Thus, the model [5] is actually a two parameter (p, Λ) family of models, with p controlling the sparsity of the network (and p^{-1} controlling the strength of its connections) and Λ controlling the % of NMDA to AMPA conductances.

3.3.1. Question 1: Orientation selectivity of complex cells. A study of this two parameter (p, Λ) family of large-scale neuronal networks [5] found that sparsity indeed stabilizes the high gain network and produces complex cells with realistic orientation selectivity, including contrast invariant tuning curves that are relatively invariant with respect to the neuron's distance in the cortical layer from pinwheel centers, as shown in Figure 3.6. Note that this network is very sparse, with p = 0.023; thus, each of the $N = 4000$ neurons is connected, on average, to only $N_{eff} = pN = 96$ neurons, but with strong PSPs scaling as p^{-1}.

3.3.2. Question 2: A high gain, stable network: Figure 3.7 shows the firing rate gain curves (as a function of the LGN drive G_{input}) for different levels of sparsity and different percentages of NMDA, for a somewhat idealized network of 1600 neurons. (See Methods in [5] for specifics about the idealization.) Figure 3.7 clearly shows that as sparsity increases, or the percentage of NMDA decreases, bistability is eliminated and the firing rates are reduced. This stabilization results from a significant increase in the level of intrinsically generated fluctuations as sparsity increases or percentage of NMDA decreases. This model works well with parameters for which the gain curves of Figure 3.7 are just below the critical value for the onset of bistability. For example, $(\Lambda = 0., p_{cr} = 0.03; N_{eff} = p_{cr} N = 50)$; that is, very sparse connectivity.

3.3.3. Question 3: The natural operating point of this high gain network. The "operating point" or "operating state" of the neuronal network model of [5] has

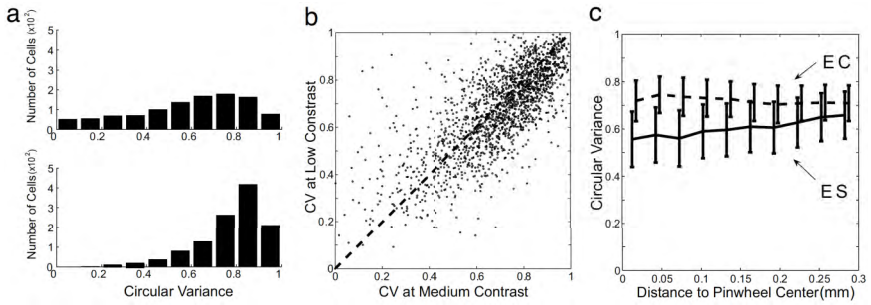

FIG. 3.6. **Orientation Selectivity of Model Excitatory Cells:** *(a) Histogram of CV for excitatory simple cells (Upper) and excitatory complex cells (Lower). (b) CV of excitatory cells at medium and low contrasts. (c) CV of excitatory cells as a function of distance to nearest pinwheel center (Solid, excitatory simple, ES; Dashed, excitatory complex, EC). Reprinted from Proc. Nat. Acad. Sci. (USA), ref [5].*

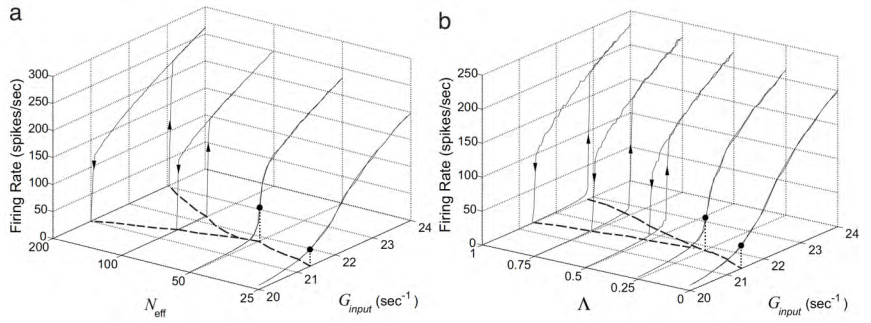

FIG. 3.7. **Bifurcation Diagrams:** *Shown is the firing rate per neuron of the excitatory cell population vs. G_{input}. These curves were obtained by first increasing and then decreasing the strength of the feedforward excitation G_{input} (a) for networks with different $N_{eff} = 25, 50, 100, 200$; [The network synaptic coupling strengths are $S_{EE}^{(s)}$ and $S_{IE}^{(s)} = 0.25$ for the simple cell population; $S_{EE}^{(c)}$ and $S_{IE}^{(c)} = 0.50$ for the complex cell population; and $S_{EI} = S_{II} = 0.9$ for all cells; $\Lambda = 0$ for each of the four cases.](b) For five networks with different $\Lambda = 0\%, 25\%, 50\%, 75\%, 100\%$, (the coupling strengths are the same as in figure (a), with $N_{eff} = 25$ for each of the five cases). Reprinted from Proc. Nat. Acad. Sci. (USA), ref [5].*

the following characteristics: It is "high-gain", just below bistability; it has large intrinsically generated fluctuations; it has large conductances, with large cortical-cortical inhibition and excitation; its total excitation (LGN + cortical-cortical) approximately balances inhibition. And its temporal fluctuations make it very asynchronous, far from either homogeneity or synchrony. An operating point with these characteristic features is very important for the [5] model to achieve and faithfully represent experimentally observed performances, such as complex cells that are well tuned for orientation, with reasonable firing rates. Sparsity of connections seems necessary to achieve and stabilize this asynchronous, high gain operating point.

One final remark about this sparse model and the egalitarian model of Section 3.2: The temporal fluctuations in both models exhibit "gamma band" behavior in that their power spectra have broad frequency bands in the gamma range between (40Hz, 100Hz), centered near 80Hz [unpublished]. These "oscillations" were observed in the spike rasters, the network firing rates, and in individual voltage traces. They were weaker in the sparse model than in the egalitarian model, because the sparse model's

operating point was more asynchronous. Numerical experiments [unpublished] were performed at different parameter values in an effort to eliminate this gamma band, or at least reduce its presence – but to no avail. This gamma band seemed robust, in both models. At the time, the authors of [4, 5] did not understand how this gamma band behavior arose in the models, and no analysis of it was performed on either model. Analysis of gamma-rhythms was carried out over a decade later by Chariker, Shapley and Young [27] for their comprehensive model described in Section 3.5. However, the robust presence of gamma band in the two earlier models did lead the authors of [4,5] to reconsider, and take more seriously, the possibility of the presence of gamma behavior in monkey V1 – another type of consequence of large-scale modeling.

3.4. Model of larger cortical patch, with long-range connections. Questions to be addressed: After exploring the potential regimes associated with a small cortical patch (e.g., a few hypercolumns within 1 square mm of cortex), [6] and [7] enlarged the scale of the model. (See also [32] for a similar model for awake, rather than anesthetized, monkey V1.) This larger model spanned $6mm \times 4mm$ of cortex, comprising $\sim$100 hypercolumns. Notably, this larger network included additional physiological features which come into play at these larger spatial scales. As discussed below, the larger network includes (a) 'long-range' synapses which connect hypercolumns several mm apart, and (b) an NMDA-type excitatory conductance with a slow decay timescale ($\sim 100ms$). Is the enlarged model sufficiently rich to exhibit the following two experimental phenomena which are observed within the cortex at these scales:

i) Spontaneous Background Patterns [6]: When unstimulated, cortical dynamics exhibits coherent spatiotemporal correlations, which can be imaged with voltage sensitive dyes [23]. These spatiotemporal correlations involve co-activity spanning multiple neuronal populations up to several mm apart, and persist with a timescale of $\sim 100ms$. Intriguingly, these spontaneous background patterns are similar in structure to the patterns of activity observed under drifting-grating stimuli; i.e., orientation-domains of similar orientation-preference tend to be active simultaneously even when separated by several mm – except that, in background, the spatial patterns exhibit irregular temporal jumps.

ii) Preattentive Illusory Motion [7]: When stimulated by a small visual 'cue' that steadily drifts (over $\sim 100ms$), the cortex responds with a burst of activity which is initially localized around the cortical footprint of the initial cue, and which then steadily spreads out to encompass the cortical footprint of the cue's trajectory (see Figure 3.8A). As visualized by voltage sensitive dyes [24], this cortical activity pattern is quite similar (both in shape and time-course) to the cortical response associated with the Hikosaka Line Motion Illusion (LMI), which is stimulated by a brief ($\sim 30ms$) visual 'cue' which abruptly transforms into a larger 'bar' (see Figure 3.8D). Note that, while the cortical response to the LMI-stimulus is similar to that evoked by the steadily-moving stimulus, the LMI-stimulus itself does not contain any actual moving image. Nevertheless, psychophysical experiments indicate that the LMI-stimulus produces the *perception* of motion, suggesting that certain kinds of visual processing may depend on the spatio-temporal dynamics of the cortical response within V1.

Note that both of these phenomena describe the behavior of large swathes of neurons across long stretches of time. Together, these phenomena pose a serious constraint on the dynamics of the enlarged model network, requiring certain kinds of coordination across different hypercolumns for several hundred *ms* at a time.

One of the main goals of study of the enlarged model was to determine the mech-

anisms at play in the large-scale model, and to understand how those mechanisms give rise to the phenomena above. Work was focused on the role played by (a) long-range connections between different hypercolumns, and (b) the slow excitatory NMDA-type conductance.

Overview of the Model: A large-scale model of a $6mm \times 4mm$ patch of V1 cortex was constructed using a two-dimensional lattice of $\sim 10^6$ model neurons, each obeying integrate-and-fire equations as in Section 2. Note that the enlarged model does not distinguish between the input-layer and the superficial layers of V1: it is an effective or "lumped" model of V1. This model cortex is driven by background noise and a model LGN (mLGN). Similar to before, the model contains $\sim 80\%$ excitatory neurons and $\sim 20\%$ inhibitory neurons, half of which receive direct mLGN input (i.e., 'simple' cells), whereas the other half do not (i.e., 'complex'); in addition, each neuron also has a preferred orientation θ (laid out in predetermined pinwheel-patterns) which is imposed by the mLGN input for that neuron. The local cortical circuit contained only AMPA, with no NMDA (although the absence of NMDA was not essential to the model's performance). The local circuit was sparsely connected, although not at the extreme sparsity level of the model of Section 3.3. The local connections had the following sparsity levels: $E \to E - -25\%; E \to I - -25\%; I \to E - -75\%; I \to I - -75\%$.

i) Long-range connections: In addition to the typical local connections described in Section 2, each excitatory neuron in the enlarged model also projects to many neurons in other more distant hypercolumns. These long-range connections are orientation-specific, and preferentially connect neurons of similar θ (as indicated experimentally in [25]). The long-range connections are chosen to be random and sparse; for any given θ, the long-range spatial coupling kernel takes the form of an anisotropic Gaussian with a spatial scale of $\sim 1.5mm$ and an eccentricity of ~ 1.5.

ii) Slow NMDA-type conductance: In addition to the faster $\sim 2ms$ AMPA excitatory conductances described in Section 2, each excitatory neuron also gives rise to a slower NMDA excitatory postsynaptic conductance with a longer decay time-constant (i.e., $\sim 100ms$). In the long range connections, the ratio of NMDA to AMPA was set at 75% NMDA to 25% AMPA, with the coupling-strength associated with the NMDA-conductance chosen so that the total postsynaptic NMDA current is roughly the same order of magnitude as the postsynaptic excitatory AMPA currents. The actual percentages of NMDA vs AMPA was not important; but the presence of NMDA was essential to the model's performance. In the long range connections, NMDA targeted both excitatory and inhibitory neurons, with inhibition more substantially targeted.

As mentioned above, the architecture of this large-scale model is endowed with two spatial scales – a small scale describing the local connections, and a significantly larger scale describing the long-range connections. In order to simulate this large system efficiently, [8] developed a fast numerical algorithm which takes advantage of this separation in scale, reducing the overall computational burden by an order of magnitude.

Results: The enlarged large-scale model derives many of its properties from its operating point. Parameters were chosen so that (i) the membrane-potential of most neurons in the network hovers close to threshold most of the time, and (ii) the excitatory and inhibitory synaptic coupling strengths are both strong. These effects create a fluctuation driven regime with a high gain; a relatively small increase in either excitatory or inhibitory current can give rise to large increases or decreases in activity.

Because many neurons tend to accumulate close to the firing-threshold, any excitatory spike can easily cause several other nearby excitatory neurons to fire shortly

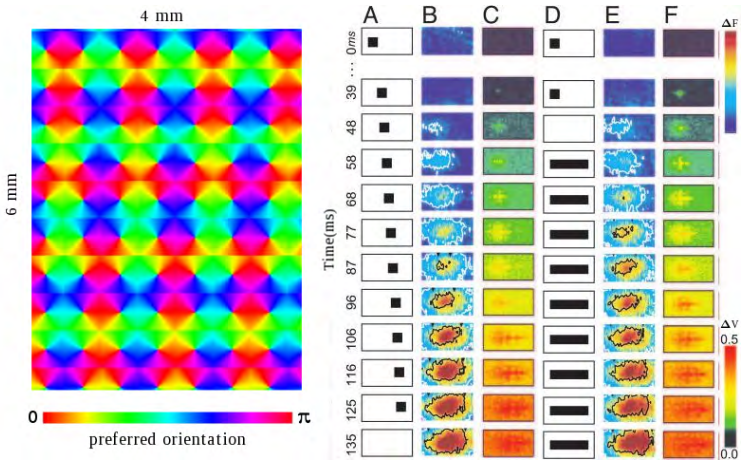

FIG. 3.8. *Large-scale model in [6, 7]. On the left we show the dimensions of the large-scale model; each pixel is colored according to its preferred orientation. On the right we show several panels, each row corresponding to a different time following stimulus onset. Column A shows a moving stimulus (presented as input to the mLGN). Column B shows the ΔF fluorescence response obtained in experiment (see [24]). Column C shows the subthreshold voltage response ΔV obtained in our model. Columns D,E,F are analogous to A,B,C, except for the LMI-stimulus. Note that, even though the image-frames in column-D change abruptly, the dynamical response of the cortex shown in Columns E,F changes continuously, similar to that shown in Columns B,C, respectively. Reprinted from [6, 7].*

afterwards. The firing of these next neurons can lead to yet more firing-events, causing a cascade that recruits a large pool of local excitatory and inhibitory neurons, with the activation of the latter curtailing any further spikes in the sequence [6]. These rapid semi-synchronous cascades will be referred to as 'recurrent-firing-events', or RFEs.

Within the context of this large-scale model, RFEs are not uncommon, comprising a small (but significant) portion of the total number of firing-events. In background the RFEs tend to be small, involving a small subset of the neurons in a local cluster. Under drive the RFEs can be larger, with the largest RFEs comprising a significant fraction of the neurons in an orientation domain.

Analysis of the large-scale network suggests that RFEs are a critically important ingredient in modeling i) spontaneous background patterns [6] and ii) the line-motion illusion [7]. To see why, first note that, whenever an RFE occurs, it tends to run its course rather quickly ($\lesssim 10ms$). This is because the transient dynamics of the RFE are controlled primarily by the fast timescales associated with the AMPA- and GABA-conductances. Nevertheless, once an RFE has concluded, the effects of the NMDA are much longer lasting. More specifically, the excitatory neurons that participated in any RFE leave their postsynaptic targets with a residual NMDA-conductance that persists for $\sim 100ms$. This residual NMDA-conductance serves to 'prime' those postsynaptic neurons: While not strong enough to cause an abundance of postsynaptic firing-events, the increased NMDA conductance does increase the subthreshold-voltage of the postsynaptic neurons. This increase in subthreshold-voltage pushes the neurons closer to the firing-threshold, increasing the probability that they will nucleate another RFE within the next 100ms or so. It is this NMDA-facilitated priming, together with the anisotropic architecture of the long-range connections, which is responsible for the large-scale phenomena in our model.

Spontaneous Background Patterns: In background any excitatory firing-event

which triggers RFEs primes not only the other nearby neurons within the same hypercolumn (via local connections), but also neurons in other hypercolumns (via long-range connections). Because the long-range connections are more common between neurons of similar orientation-preference, RFEs tend to prime multiple orientation domains of similar orientation preference simultaneously. The spatial extent of these spontaneous patterns is linked to the scale of the long-range connections, which span several *mm* of cortex. These spontaneous background patterns themselves are similar to the patterns of cortical activity driven by oriented grating stimuli, except they do not persist very long temporally. Rather, these background patterns decay and are re-initiated, irregularly in time and randomly in orientation, by the next collection of RFEs.

Preattentive Illusory Motion: Under the LMI-stimulus, the initial cue causes vigorous cortical firing along with several RFEs in the cortical footprint of the cue. These RFEs then prime the neighboring cortex, with a spatial profile that extends beyond the cue, but not so far as to encompass the entire cortical footprint of the bar to follow. Subsequently, when the LMI-stimulus changes from cue to bar, the primed area of cortex (closer to the original cue) responds before the more distal unprimed areas (at the far end of the bar). This staggered response gives rise to a spatiotemporal dynamic profile similar to that observed under a growing stimulus (see Figure 3.8B,C and 3.8D,E).

In summary, investigations of the enlarged large-scale model highlighted once again the importance of recurrent synaptic interactions. Specifically, the interplay between neurons in a high-gain state naturally facilitates rapid causal sequences of firing-events – i.e., recurrent-firing-events. These RFEs serve as dynamical building blocks which lay the foundation for more complicated large-scale phenomena.

3.5. A new model of macaque V1: From structure to dynamics to function. A few years ago, Logan Chariker (then PhD student), Robert Shapley, and Lai-Sang Young embarked on a project to study macaque V1 cortex through computational modeling. This problem had been tackled by several groups at NYU in the 1990s and early 2000s (see [2, 4] and the references therein). Young's group benefited from this earlier research; indeed they used as their starting point a number of ideas from [4]. The present effort has a strong focus on population dynamics not present in previous studies. To discover mechanisms they would study not only behaviors of individual model neurons but also how neurons in a population interact dynamically with one another, and their experience has convinced them that analysis of population activity in large-scale network models has the potential to yield new and valuable information for neuroscience.

Two pieces of modeling work below illustrate (i) how structure and dynamics are connected to function and (ii) the rich interplay between neuroscience and mathematics. The reader is referred to published papers for a more systematic treatment.

Model overview. The primary target of the model is a small region of Layer 4Cα (L4), the input layer to V1 in the magnocellular pathway of the macaque visual cortex. In addition to L4, the model has two other components: the thalamic Lateral Geniculate Nucleus (LGN), which feeds forward to L4, and Layer 6 (L6) in V1, which feeds back to L4. The physical layout of the model is depicted in Figure 3.9A.

This model has been challenged with an ensemble of visual stimuli consisting of drifting gratings of many orientations, spatial frequencies and contrasts, and has passed all the tests, producing outputs that closely resembled experimental data. These tests include firing rates, tuning curves, contrast response functions, contrast dependence, both

on the level of individual neurons and on populations. The model also produces simple and complex cells; it produces diverse neuronal responses and gamma-band rhythms, to name some of its main properties. The problem of feedback, a perennial headache for modelers, is solved in this model with a self-adjusted dynamic algorithm. This scheme, which will appear in a forthcoming paper, has greatly expanded the versatility of the model.

All model results were achieved in a single model, using a single set of parameters. This is important, for as mentioned earlier, one of the primary goals of Young and colleagues is to uncover mechanisms, and the wider the range of V1 phenomena a model is able to replicate, the more confident one can be that model function is derived from mechanisms similar to those in the real cortex.

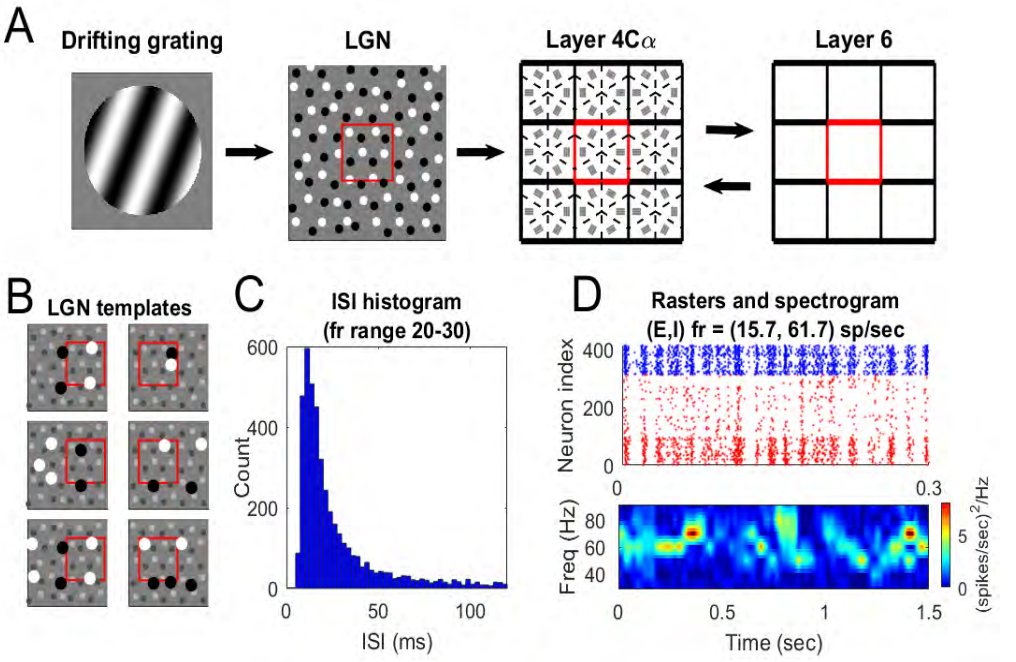

FIG. 3.9. **A. Model layout.** *The grating on the left is symbolic of the visual stimulus presented to the eye. LGN is modeled as ON/OFF cells, the red square at the center of the LGN sheet corresponding roughly to one Hypercolumn (HC) in cortex. LGN projects to Layer 4Cα. The right half of the diagram depicts a feedback loop between Layer 4Cα and Layer 6. The model has 9 HC each subdivided into 6 intended orientation domains; a majority of the neurons in each domain is connected to LGN configurations spatially aligned with the intended orientation.* **B. LGN templates.** *Shown are 3 admissible LGN configurations for 4Cα cells in the vertical-preferring domain (left), horizontal-preferring domain (right).* **C. Interspike intervals.** *Shown are ISI plots of 10 E-neurons with firing rates between 20-30 spikes/s superimposed.* **D. Gamma-band activity.** *Top: Rasters of spikes of cells in a patch of 400 E- and and I-cells in the vertical-preferring domain of the central HC. These are spike time rasters during stimulation by an optimal grating, drifting at 4 Hz. The x-axis is time; y-axis is neuron index within the patch. E cell spikes are red dots, sorted by decreasing number of LGN inputs: the cells near the bottom are likely complex; I cell spikes are blue dots. Bottom: Time-frequency analysis of spike density. Power spectral density is calculated within sliding windows of 200 ms, for the same data as shown in the raster. The color plot shows wandering frequencies centering at around 60 Hz.*

Orientation selectivity from sparse LGN inputs. The following example shows

how Young et al. made an effort to adhere to neuroanatomy (structure), and to explain the simulation results (function) that followed. The results are reported in [9].

Hubel and Wiesel proposed that orientation selectivity (OS) for a V1 neuron is derived from the alignment of its LGN afferents. The number of LGN inputs to a V1 cell at $\sim 5^\circ$ eccentricity was previously assumed to be 15-30 [2, 4, 5, 7]. When Young et al. tried to put the model together, they had difficulty reconciling these numbers with the sizes of LGN receptive fields and their amount of overlap. This caused them to search the literature, and to discover that a number of earlier experiments had in fact pointed to a significantly smaller of LGN inputs [26, 28, 29].

Constrained by the small number (9-10) of LGN cells per hypercolumn, the reach of each LGN cell, the requirement that there be rows of ON and OFF cells aligned in various directions, and the distances between rows required to satisfy preferred spatial frequencies, Young and colleagues were confronted with a perplexing geometric-combinatorial problem. Using a perturbed hexagonal lattice, they found that this problem in fact had solutions, though barely. Examples of admissible LGN configurations are shown in Figure 3.9B.

The sparseness of LGN led immediately to the following question: is this really enough to confer OS on V1 cells? With an average of 3-4 LGN inputs per V1 cell, the feedforward current is necessarily small ($\sim 10\%$ of the total excitatory current received by E-neurons in Layer 4Cα), contradicting traditional feedforward views. One might question also the number of distinct orientations that can be formed out of such a small pool of LGN cells, or the effectiveness of rows of 2-3 ON/OFF LGN cells in constraining orientation.

The model in [9] dispelled once and for all these concerns. The model described there was able to produce distributions of firing rates for E and I cells that emulated data, in background as in drive, in optimally as well as in orthogonally driven regions of cortex. In the model while LGN currents were broad and weak, consistent with the numbers and geometry above, cortico-cortical interactions magnified and sharpened OS of neurons in V1. The sparseness of LGN is an important difference between [9] and models by earlier NYU groups. Another departure from previous NYU models is that they have used realistic connectivities between E- and I-cells based on data.

Interspike intervals (ISI) and gamma-band rhythms. Gamma-band activity is an emergent phenomenon in neuronal systems. Together with ISI, it is also an example of how individual and collective dynamical behaviors of neurons can be very different.

The ISI of Excitatory neurons are well known to have distributions resembling those of exponential random variables; see Figure 3.9C. Yet throughout cortex, one observes that, when stimulated, local populations produce a rhythm in the gamma band; see Figure 3.9D (top). These two very different spiking patterns may at first sight appear to contradict one another, but they do not: Comparing the firing rates of individual neurons to the frequencies of the spiking events in Figure 3.9D, one sees that most neurons participate in only a fraction of the events, and their ISI plots show that the participation is irregular, skipping random numbers of events before participating in another one.

As to how gamma rhythms are produced, the first explanation was a model called PING [31]. PING produces regular oscillations fueled by full E-population spikes driving full I-population spikes, the cycle repeating when the suppression ends. Several years ago, [30] proposed the idea of multiple-firing events (MFEs): Fluctuations under drive cause a few E-neurons to cross threshold. That may or may not produce enough recurrent excitation to cause more E and I-neurons to spike. If that happens, it will

be followed by a commensurate pushback by I-cells milliseconds later. The decay of I-conductance and depolarization of E-cells then completes the cycle. The idea has similarities with PING, but only fractions of the population are involved, variable fractions of E and I neurons depending on their operating points and to some degree sheer "luck". MFEs as a concept are not the same as RFEs referred to in Section 3.4, which consist of recurrent single bursts of E-firing separated by timescales of total inactivity of the E-population lasting the full duration of NMDA, i.e. 100 ms. RFE's are analyzed in [30] (Figure 9 in Supp. Info.), where it is seen that they differ substantially from MFEs like those shown in panel Figure 3.9D.

The model in [9] produces a gamma-rhythm when driven by a drifting grating. It is an emergent phenomenon; nothing was programmed into the model to make that happen. Young et al. studied this rhythm in more detail in [27], and found a remarkable resemblance between it and real data: the rhythm is episodic, graded in power, and wandering in phase and frequency; see Figure 3.9D (bottom). Young et al. used this model to investigate underlying mechanisms, and found that what drives gamma-band activity in the model is much closer to the MFEs described in [30] than to PING; in particular, it is driven more by recurrent excitation than by disinhibition. That, however, was not the whole story: while gamma-band activity is generated within local populations, they also found that pulses from regions outside of the local population have a stronger than expected influence on this rhythm.

4. Conclusion

Our work shows that today enough is known to make comprehensive models of the primary visual cortex that emulate its function in great detail, quantitatively. This is particularly established by the latest comprehensive large-scale models of references [9,27]. Future work will lead, we hope, to more experiments and better models – toward a better understanding of what the visual cortex is trying to do.

REFERENCES

[1] R. Ben-Yishai, R. Bar-Or, and H. Sompolinsky, *Theory of orientation tuning in visual cortex*, Proc. Natl. Acad. Sci. USA, 92:3844–3848, 1995. 1

[2] D. McLaughlin, R. Shapley, M. Shelley, and D. Wielaard, *A neuronal network model of macaque primary visual cortex (V1): orientation selectivity and dynamics in the input layer* $4C\alpha$, Proc. Natl. Acad. Sci. USA, 97:8087–8092, 2000. 1, 3.1, 3.1, 3.1.2, 3.2, 3.1.3, 3.5, 3.5

[3] D. Wielaard, M. Shelley, D. McLaughlin, and R. Shapley, *How simple cells are made in a nonlinear network model of the visual cortex*, J. Neurosci., 21(14):5203–5211, 2001. 1, 3.1, 3.1.3, 3.2.1

[4] L. Tao, M. Shelley, D. McLaughlin, and R. Shapley, *An egalitarian network model for the emergence of simple and complex cells in visual cortex*, Proc. Natl. Acad. Sci. USA, 101:366–371, 2004. 1, 3.3, 3.2.1, 3.4, 3.5, 3.3, 3.3, 3.3.3, 3.5, 3.5

[5] L. Tao, D. Cai, D. McLaughlin, M. Shelley, and R. Shapley, *Orientation selectivity in visual cortex by fluctuation-controlled criticality*, Proc. Natl. Acad. Sci. USA, 103:12911–12916, 2006. 1, 3.3, 3.3, 3.3.1, 3.3.2, 3.3.3, 3.6, 3.7, 3.5

[6] D. Cai, A. Rangan, and D. McLaughlin, *Architectural and synaptic mechanisms underlying coherent spontaneous activity in V1*, Proc. Natl. Acad. Sci. USA, 102:5868–5873, 2005. 1, 3.4, 3.8, 3.4

[7] A. Rangan, D. Cai, and D. McLaughlin, *Modeling the spatio-temporal cortical activity associated with the line-motion illusion in the primary visual cortex*, Proc. Natl. Acad. Sci. USA, 102:18793–18800, 2005. 1, 3.4, 3.8, 3.4, 3.5

[8] A. Rangan and D. Cai, *Fast numerical methods for simulating large-scale integrate-and-fire neuronal networks*, J. Comput. Neurosci., 22:81-100, 2007. 3.4

[9] L. Chariker, R. Shapley, and L-S. Young, *Orientation selectivity from very sparse LGN inputs in a comprehensive model of macaque V1 cortex*, J. Neurosci., 36(49):12368–12384, 2016. 1, 3.5, 4

[10] D. Hubel and T. Wiesel, *Receptive fields, binocular interaction and functional architecture in the cat's visual cortex*, J. Physiol., 160:106–154, 1962. 3.2

[11] E. Benardete and E. Kaplan, *The dynamics of primate m retinal ganglion cells*, Visual Neurosci., 16:355–368, 1999. 2

[12] C. Beaulieu, Z. Kisvarday, P. Somogyi, M. Cynader, and A. Cowey, *Quantitative distribution of GABA-immunopositive and immunonegative neurons and synapses in the monkey striate cortex (Area 17)*, Cereb. Cortex, 2:295–309, 1992. 2

[13] H. Sompolinsky and R. Shapley, *New perspectives on the mechanisms for orientation selectivity*, Curr. Opin. Neurobiol., 7:514–522, 1997. 3.1

[14] K. Obermayer and G. Blasdel, *Geometry of orientation and ocular dominance columns in monkey striate cortex*, J. Neurosci., 13:4114–4129, 1993.

[15] F. Mechler and D. Ringach, *On the classification of simple and complex cells*, Vision Res., 42(5):1017–1033, 2002. 3.2.3

[16] L. Abbott and F. Chance, *Rethinking the taxonomy of visual neurons*, Nat. Neurosci., 5(5):391–392, 2002. 3.2.3

[17] N.J. Priebe, F. Mechler, M. Carandini, and D. Ferster, *The contribution of spike threshold to the dichotomy of cortical simple and complex cells*, Nat. Neurosci., 7(10):1113–1122, 2004. 3.2.3

[18] D. Ringach, M. Hawken, and R. Shapley, *Dynamics of orientation tuning in macaque primary visual cortex*, Nature, 387:281–284, 1997. 3.1.2, 3.2, 3.5

[19] D. Ringach, R. Shapley, and M. Hawken, *Orientation selectivity in macaque V1: diversity and laminar dependence*, J. Neurosci., 22(13):5639–5651, 2002. 3.1.1

[20] J. Movshon, I. Thompson, and D. Tolhurst, *Receptive field organization of complex cells in the cat's striate cortex*, J. Physiol., 283:79–99, 1978. 3.1.3

[21] R. De Valois, R. Albrecht, and D. Thorell, *Spatial frequency selectivity of cells in macaque visual cortex*, Vision Res., 22:545-559, 1982. 3.1.3

[22] J. Alonso, W. Usrey, and R. Reid, *Rules of connectivity between geniculate cells and simple cells in cat primary visual cortex*, J. Neurosci., 21:4002–4015, 2001. 3.1

[23] M. Tsodyks, T. Kenet, A. Grinvald, and A. Arieli, *Linking spontaneous activity of single cortical neurons and the underlying functional architecture*, Science, 286:1943–1946, 1999. 3.4

[24] D. Jancke, F. Chavance, S. Naaman, and A. Grinvald, *Imaging cortical correlates of illusion in early visual cortex*, Nature, 428:423–426, 2004. 3.4, 3.8

[25] W. Bosking, Y. Zhang, B. Schofield, and D. Fitzpatrick, *Orientation selectivity and the arrangement of horizontal connections in tree shrew striate cortex*, J. Neurosci., 17:2112–2127, 1997. 3.4

[26] A. Angelucci and K. Sainsbury, *Contribution of feedforward thalamic afferents and corticogeniculate feedback to the spatial summation area of macaque V1 and LGN*, J. Comp. Neurol., 498:330–351, 2006. 3.5

[27] L. Chariker, R. Shapley, and L.-S. Young, *Rhythm and synchrony in a cortical network model*, J. Neurosci., 38:8621–8634, 2018. 1, 3.3.3, 3.5, 4

[28] M. Connolly and D. Van Essen, *The representation of the visual field in parvicellular and magnocellular layers of the lateral geniculate nucleus in the macaque monkey*, J. Comp. Neurol., 226:544–564, 1984. 3.5

[29] L.C.L. Silveira and V.H. Perry, *The topography of magnocellular projecting ganglion cells (M-ganglion cells) in the primate retina*, Neurosci., 40:217–237, 1991. 3.5

[30] A.V. Rangan , and L.-S. Young, *Emergent dynamics in a model of visual cortex*, J. Comput. Neurosci., 35:155–167, 2013. 3.5

[31] M.A. Whittington, R.D. Traub, N. Kopell, B. Ermentrout, and E.H. Buhl, *Inhibition-based rhythms: experimental and mathematical observations on network dynamics*, Int. J. Psychophysiol, 38:315–336, 2000. 3.5

[32] D. Zhou, A. Rangan, D. McLaughlin, and D. Cai, *Spatiotemporal dynamics of neuronal population response in the primary visual cortex*, Proc. Natl. Acad. Sci. USA, 110(23):9517–9522, 2013.

1, 3.4